3

Aegle marmelos leaf-based SERS platform for detection and quantification of antibiotics in milk

Present chapter illustrates the utilization of naturally found aegle marmelos (AM) leaf as a highly sensitive SERS platform. The proposed SERS substrate has been obtained through surface adsorption of AuNPs on the roughened microstructured pattern of the AM leaf. The morphological patterns and the dimension of the synthesised AuNPs have been characterised by FESEM and TEM. The performance of the proposed SERS substrate has been initially evaluated through detection of standard Raman active samples and upon noticing reliable performance, its applicability has been demonstrated by detecting antibiotics in cow milk. An optimized ML-based classification model has been proposed for rapid identification of analyte molecules in real milk samples.

3.1 Introduction

Naturally available micro or sub-microstructured surfaces offer an excellent platform for creating electromagnetic hotspots upon surface adsorption of noble metallic nanoparticles like gold or silver. Amongst these, leaf structures are particularly intriguing due to their widespread availability and micro-structured morphology. Various leaf-based nanostructures have already found applications across various domains, with a recent focus on developing hydrophobic SERS substrates [1, 2]. These substrates facilitate the aggregation of metal nanoparticles within a confined area, leading to enhanced SERS signals from localized regions. However, a common challenge with such substrates is the uneven distribution of SERS signals. To address this, the present work propose the use of hydrophilic SERS substrates to achieve uniform signal distribution over large area. In the current study, a sensitive and cost-effective SERS platform was fabricated by decorating AuNPs on *AM* leaf surfaces for the detection and analysis of Raman-active samples. The usability of this sens-

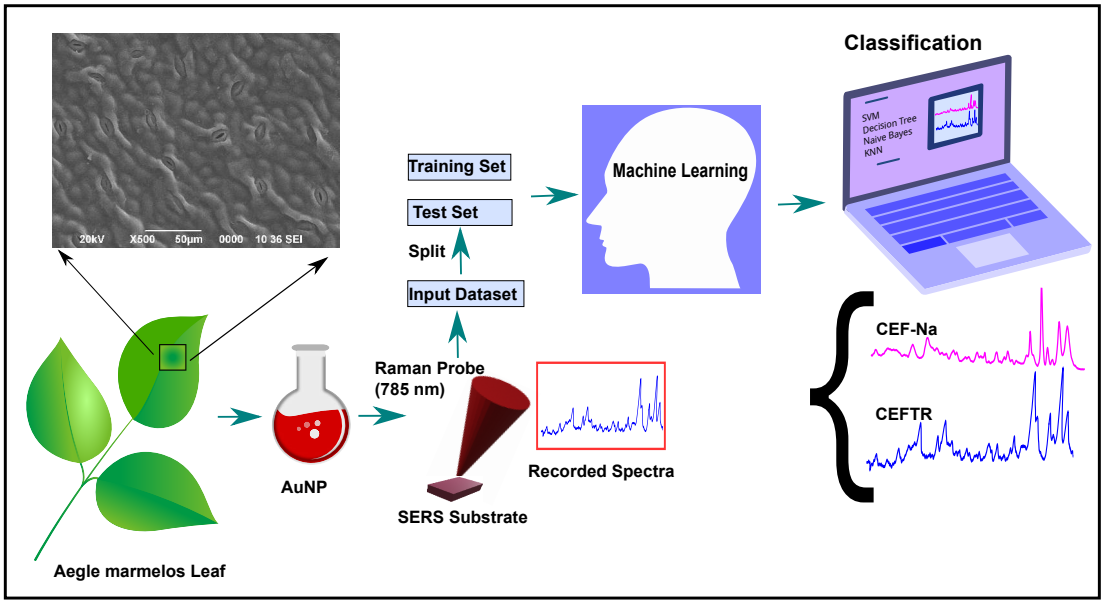

Figure 3.1: Schematic of the proposed sensing work

ing platform was demonstrated by detecting two antibiotics, CEFTR and CEF-Na, in cow milk samples. With the proposed SERS substrate, the detection of targeted analytes can be carried out at concentrations as low as 0.1 ppm with reasonably high reproducibility. Figure 3.1 outlines the schematic of the proposed leaf-based sensing approach.

In SERS, the surface morphology of the substrate plays a crucial role in signal fluctuations and enhancement of the scattered Raman signals from the sample. The uniform deposition of AuNPs over the surface facilitates relatively stable SERS signal intensity recorded from the substrate. An ML-based classification model has been implemented in the present study to classify the antibiotics used in milk samples. Prior to performing the ML, PCA was calculated for the spectral data of the present sensing platform. In the proposed spectroscopic analysis, an optimum classification accuracy of 94% has been observed with the SVM algorithm when coupled with the PCA.

3.2 Experimental

3.2.1 Chemicals

The Raman probes R6G and MG were procured from Alpha Aesar, India, while gold chloride trihydrate ($HAuCl_4 \cdot 3\,H_2O$), $AgNO_3$, $C_6H_5Na_3O_7$, and polyvinylpyrrolidone (PVP) were procured from Merck in India. CEF-Na and CEFTR were acquired from a nearby pharmacy. All chemicals were utilized without any additional processing.

3.2.2 Synthesis of AuNPs

The conventional Turkevich method [3] was utilized to produce the AuNPs, involving the reduction of auric chloride to generate the nanoparticles. In essence, 100 mL of boiling 0.1 wt% $HAuCl_4 \cdot 3\,H_2O$ was vigorously stirred with 300 µL of 1 wt% $C_6H_5Na_3O_7 \cdot 2\,H_2O$ solution. Within 15 minutes, the solution gradually transformed into a dark red hue, indicating successful AuNP formation. Subsequently, the solution was allowed to cool to room temperature. The TEM image of the synthesized AuNPs is depicted in figure 3.2(a). By analyzing figure 3.2(b), the average size of the AuNPs was estimated to be (65±17.91) nm.

3.2.3 Synthesis of AgNPs

The polyol method [4], known for producing spherical AgNPs stabilized by PVP, was employed to synthesize Ag-PVP nanoparticles. Initially, a solution comprising 1 g of PVP K30 dissolved in 20 mL of DI was heated with constant stirring. Subsequently, 1 g of $AgNO_3$ was introduced into the mixture at 80 °C, and the resulting nanoparticle solution was heated for an hour. The size of the synthesized AgNPs was estimated to be approximately (50±13) nm.

3.2.4 Fabrication of SERS substrate

Prior to fabricating the proposed SERS substrates, the *AM* leaves were treated in ethanol followed by a 5 minutes of ultrasonication in DI water and then allowed to dry in vacuum desiccator for 60 minutes at 40 °C. The dried leaves were cut into 1 cm × 1 cm pieces. 10 µM of the synthesized AuNPs and AgNPs were separately micropipetted onto the leaf surfaces. To prepare for SERS investigations, all fabricated SERS substrates were dried in a vacuum desiccator for 30 minutes. Figure 3.3 illustrates the elemental mapping of the designed SERS platform.

3.2.5 Milk samples

The milk samples were extracted using a procedure slightly different from the procedure reported by Cheng et al. [5]. To precipitate the protein, 10 mL of cow milk sample was mixed with 4 mL of acetonitrile with a pH of 4.0 and centrifuged for an additional 10 minutes at 3000 rpm. Following centrifugation, the supernatant of the solution was carefully removed and preserved for subsequent analysis.

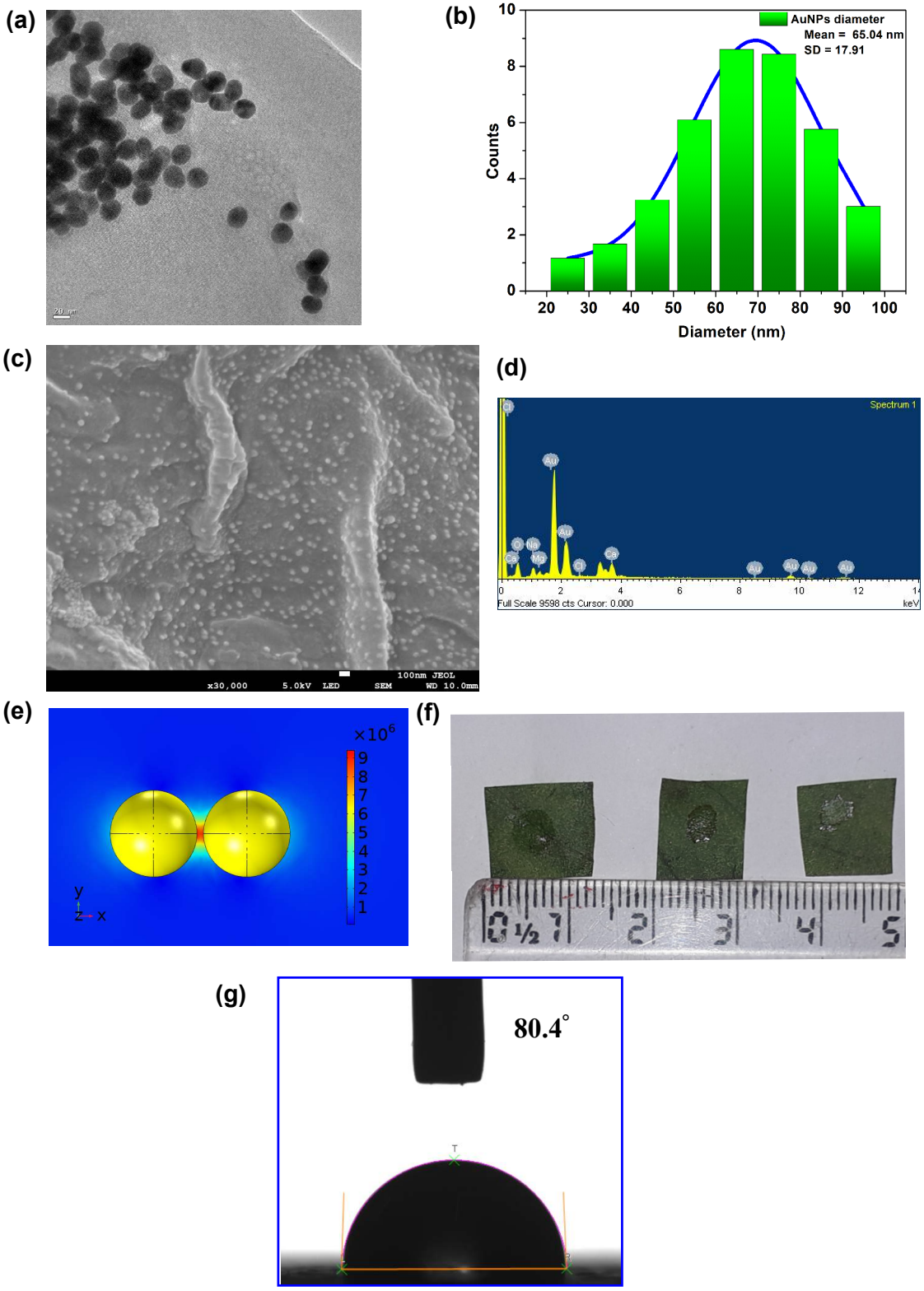

Figure 3.2: (a) TEM image of the synthesized AuNPs (Scale bar is 20 nm) (b) estimation of the mean size of the synthesized AuNPs (c) FESEM image of the designed leaf SERS substrate (Scale bar is 100 nM) (d) EDX spectra of the designed SERS substrate (e) simulation of LSPR field of generated near the hotspot region of the AuNPs distributed over leaf substrate assuming incident electric field amplitude as 6.3×10^4 Vm^{-1} (f) image of the designed SERS substrate (g) Photo image of the water droplet dispensed on the AuNP decorated leaf SERS substrate

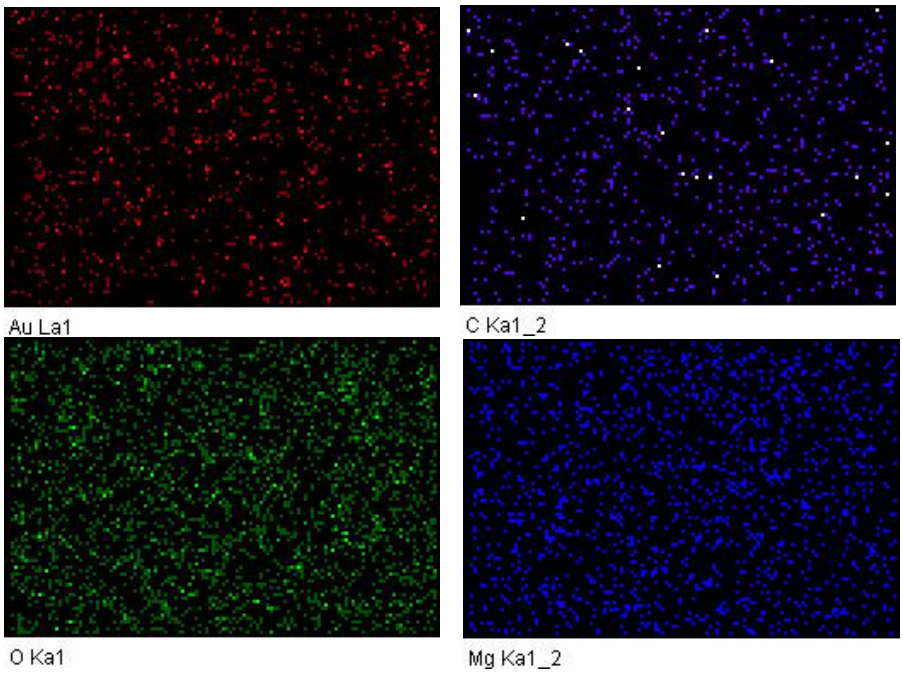

Figure 3.3: Elemental mapping of the SERS substrate indicating presence of elements

3.2.6 Raman instrumentation and Data analysis

The specification of the Raman instrument has been illustrated in the section 2.2.4. PCA and various ML algorithms were conducted using the R data analysis software [6]. SVM, decision trees, Naive Bayes, and KNN - four commonly employed ML algorithms were utilized to classify antibiotics in 200 milk samples.

3.2.7 Electromagnetic simulation

EM simulation was conducted, assuming the presence of two AuNPs on the leaf SERS substrate. In EM simulations, the assumption of a dimer system (two closely spaced particles) is often used as a simplified model to understand plasmonic behaviour, near-field enhancement, and hotspot formation. This assumption is not exact representative of the experimental nanostructures/hotspots because of geometrical complexity and material inhomogeneity of the real nanostructures. However, to get a preliminary idea of the coupled field magnitude and to reduce the total simulation time the assumption of dimer was adopted. The resonant amplitude of the EM field generated in the hotspot area of the fabricated SERS substrate was evaluated using finite element method-based software - COMSOL Multiphysics (wave-optics module). The simulation was carried out under the assumption of linearly polarized light with a wavelength of 785 nm, incident normally on the designed SERS substrate. For these simulation studies, AuNPs with dimensions of 65 nm was considered. Figure 3.2(e) illustrates the distribution of the EM field amplitude near the AuNPs, with the maximum EM field amplitude estimated at 9.2×10^6 Vm^{-1}. The incident electric

field amplitude was assumed in the simulation as 6.3×10^4 Vm^{-1}. The estimated enhancement factor from the simulation closely matches the experimentally measured value. Some variations are observed to occur due to the non ideal approximation in the simulation such as perfect geometries, homogeneous material properties, and ideal boundary conditions. The details of EF, estimated through both simulation and experimental methods, are described in table 8.16.

3.2.8 Contact angle measurement

The contact angle measurement for the proposed SERS platform was conducted using a contact angle meter (Kyowa Interface Science Co. Ltd, Japan). 4 mL water droplet was dispensed onto the surface of the AM leaf. Figure 3.2(g) illustrates the image of the water droplet dispensed over the leaf substrate for the contact angle measurement. The contact angle was determined to be 80.4 ° with a standard deviation of 1.5% over three consecutive measurements. The formation of this acute angle suggests that the fabricated surface is hydrophilic in nature. The low contact angle facilitates a uniform deposition of AuNPs across the leaf surface, as evidenced from the FESEM image depicted in figure 3.2(c).

3.3 Results and discussion

3.3.1 Optimization of the SERS substrate

At the outset of the experimental investigations, two sets of nanoparticles - AuNPs and AgNPs were considered and treated separately on the surface of AM leaf to compare the SERS spectra scattered from the SERS substrate. Figure 3.4(a) depicts the background Raman spectra of the fabricated SERS substrate. The figure clearly demonstrates that the proposed SERS method exhibits negligible background Raman signatures and does not interfere with fluorescence spectra. The fluorescence emitted from the leaf is primarily attributed to the presence of chlorophyll molecules [7], with excitation wavelengths falling within the range of 400 to 500 nm [8]. As the present sensing scheme employs a 785 nm diode laser as the excitation source, the likelihood of fluorescence emission from the AM leaf is eliminated in this study. Figure 3.4(a) shows the distinct SERS signal of MG scattered from AgNP and AuNP-treated AM leaf surfaces. It is evident that the SERS signal for the AuNP-treated leaf substrate exhibits greater sensitivity compared to the AgNP-treated counterpart. The high sensitivity of the AuNP treated AM leaf SERS substrate compared to AgNP treated counterpart is attributed to the magnitude of the coupled electro-magnetic field in the hotspots regions of the proposed SERS platform. Owing to the higher LSPR field associated with the AuNPs than AgNPs in the present experimental condition, we

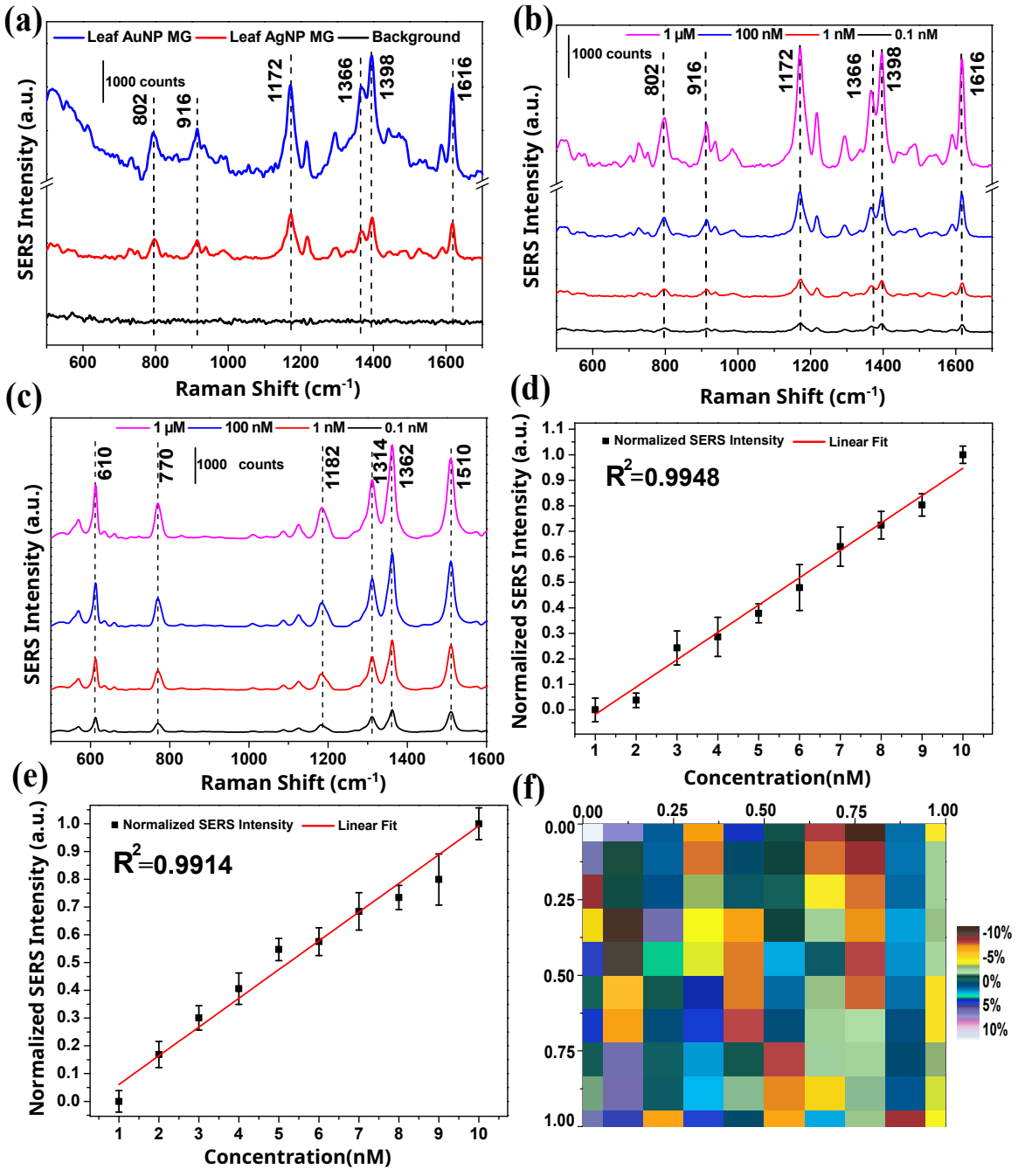

Figure 3.4: (a) SERS signature of MG for AuNP and AgNP treated leaf SERS substrate; SERS spectra of AuNP treated SERS substrate, at various concentrations (b)MG, (c) R6G, (d) linear regression analysis for the quantitative estimation of MG for the Raman band near 1398 cm^{-1} (e) linear regression analysis for the quantitative estimation of R6G for the Raman band near of 1362 cm^{-1} (f) Raman mappings of the analyte MG performed by choosing the Raman band near 1398 cm^{-1} over a matrix 10 × 10 for a sensing area of 1 mm^2; (Error bars are plotted using the standard deviation, calculated from five repetitions for each sample)

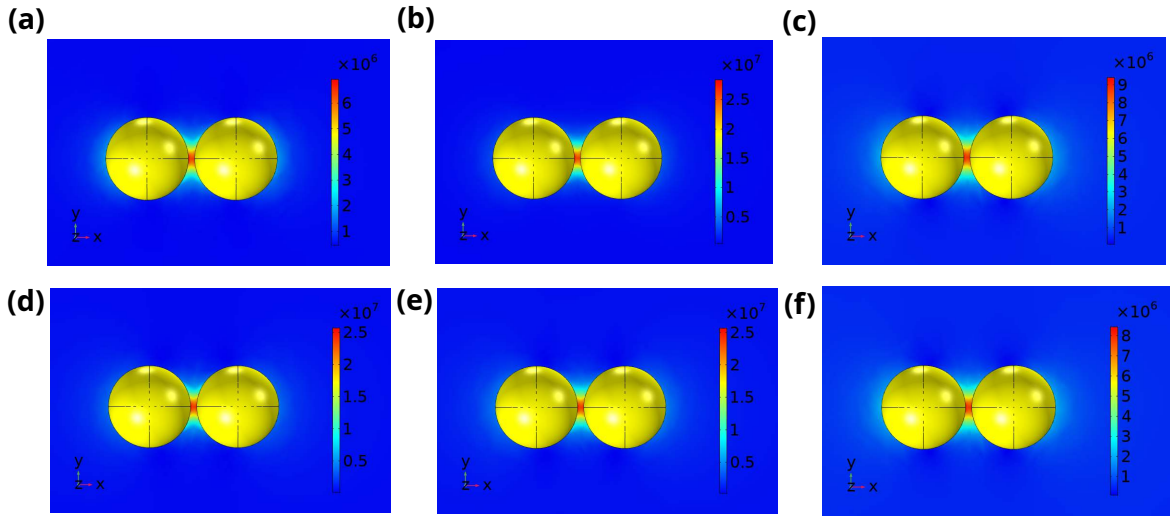

Figure 3.5: Distribution of EM field magnitude in the vicinity of AuNPs when the size of the NPs are assumed as 65 nm and separated by 5 nm with an excitation wavelength (a) 488 nm (b) 532 nm (c) 785 nm; Distribution of EM field magnitude in the vicinity of AgNPs when the size of the NPs are assumed as 65 nm and separated by 5 nm with an excitation wavelength (d) 488 nm (e) 532 nm (f) 785 nm; the incident electric field amplitude was assumed as 6.3×10^4 Vm^{-1}

noticed a relatively better SERS performance for the AuNP treated *AM* leaf substrate than AgNP treated *AM* leaf SERS substrate. EM simulation studies have been conducted to evaluate the intensity of the coupled EM field for AuNPs and AgNPs, each having an average size of 65 nm and maintaining a 5 nm separation, under various incident laser wavelengths including 488 nm, 532 nm, and 785 nm. The outcomes of these simulations studies are illustrated in tabular form in table 3.1 and are depicted in figure 3.5. Furthermore, an additional EM simulation investigation was performed to examine the influence of gap between the AuNPs on the generation of the coupled electric field. The spacing between the AuNPs plays a crucial role in determining the strength of the coupled EM field enhancement, which subsequently increases the overall SERS enhancement factor. Smaller gaps between the AuNPs result in more prominent field enhancements and, consequently, higher SERS enhancement factors. Further elaboration on this study is provided in figure 3.6.

Table 3.1: Comparison of the coupled electric field amplitude with the variation of excitation wavelength

Excitation wavelength (nm)	Material used	Gap between the NPs	Electric field (Vm^{-1})
488	AuNPs	5 nm	6.3×10^6
	AgNP		2.6×10^7
532	AuNPs		2.8×10^6
	AgNPs		2.5×10^6
785	AuNPs		9.2×10^6
	AgNPs		8.2×10^6

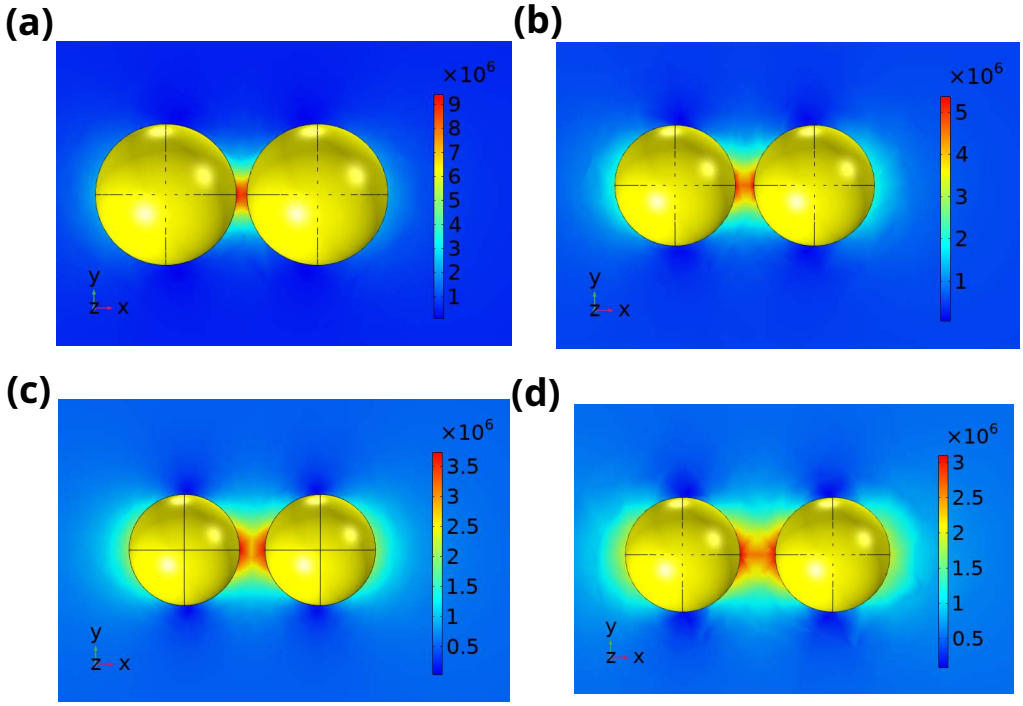

Figure 3.6: EM simulation for two AuNPs with average size 65 nm illuminated with an excitation wavelength of 785 nm when separated by (a) 5 nm (b)10 nm (c) 15 nm (d) 20 nm; the incident electric field amplitude was assumed as 6.3×10^4 Vm^{-1}

3.3.2 Characterization of the SERS substrate

To evaluate the effectiveness of the proposed SERS platform, two commonly employed SERS probe molecules, MG and R6G, were utilized for the sensing study. Initially, 1 µM of MG and R6G samples were prepared in the laboratory by dissolving appropriate amount in DI water. Three additional samples of concentrations 100 nM, 1 nM, and 0.1 nM have been derived from the stock solution by dilution with the DI water. After the sample preparation step, Raman spectra were acquired from the designed leaf substrates. Figure 3.4(b) displays the recorded spectra of MG at varying concentrations, while figure 3.4(c) illustrates the collected spectra of R6G at different concentrations, respectively. The peak assignments for MG and R6G have been provided in appendix tables 8.1 and 8.2 respectively. Regression analyses presented in figures 3.4(d) and (e) indicate a strong linear correlation between the SERS signal intensity and the concentration of the analytes. The linear correlation coefficients for MG and R6G are estimated to be R^2=0.9948 and R^2=0.9914, respectively. These high regression coefficient values suggest a good degree of linearity between the scattered Raman signal intensities and the concentrations of the analytes.

3.3.3 Evaluation of LoD

In order to calculate the LoD, the concentration range of 1 nM to 10 nM was considered. From figure 3.4(d), the LoD was calculated using the equation 2.1. The LoD of the proposed sensing platform is estimated to be 0.88 nM.

3.3.4 Uniformity characteristics

The uniformity characteristics was studied by mapping Raman peak of MG at 1398 cm^{-1} for a matrix of 10 × 10 over a sensing region of 1 mm^2. Figure 3.4(f) depicts the variation in the intensity of SERS spectra of MG near the Raman band 1398 cm^{-1}. For the considered sensing region, a maximum fluctuation of 10% was observed in the SERS signal intensity indicating a high degree of uniformity.

3.3.5 Time evaluation and reproducibility study

In the following step, the temporal performance of the proposed SERS platform was evaluated. Figure 3.7(a) depicts the changes in the scattered Raman signal strength for the Raman bands near 1172 cm^{-1}, 1398 cm^{-1}, and 1618 cm^{-1} of MG recorded by the spectrometer for a period of 10 days. A relatively stable SERS signals have been observed for the first seven days and after that signal intensity gradually started to degrade. The reproducibility characteristic of the proposed *AM* SERS substrate was also evaluated. 10 µL of 1 µM MG and R6G were drop-casted separately over ten different prepared lead substrates. The average scattered Raman signal intensity was collected from the seven random locations from each SERS substrate. Figures 3.7(b) and 3.7(c) depict the reproducibility characteristics of the proposed SERS substrate. For MG, the maximum values of RSD near the Raman bands 1172 cm^{-1}, 1398 cm^{-1} and 1618 cm^{-1} are observed to be 4.32%, 5.13% and 4.57%, respectively while for R6G these values at 770 cm^{-1}, 1362 cm^{-1}, 1510 cm^{-1} are found to be 4.39%, 4.21% and 4.65% respectively. The low RSD values infer that the fabricated substrate yields a high reproducibility characteristics.

3.3.6 Estimation of EF

The EF of the developed SERS substrate was evaluated using equation 2.2 and following the procedure already described in section 2.3.4. For MG and R6G the EF values have been estimated separately and presented in tabular form in table 3.2.

A comparison of the present sensing scheme with some previously reported literature and the current leaf SERS substrate for the sensing of various chemicals is summarized in table 3.3.

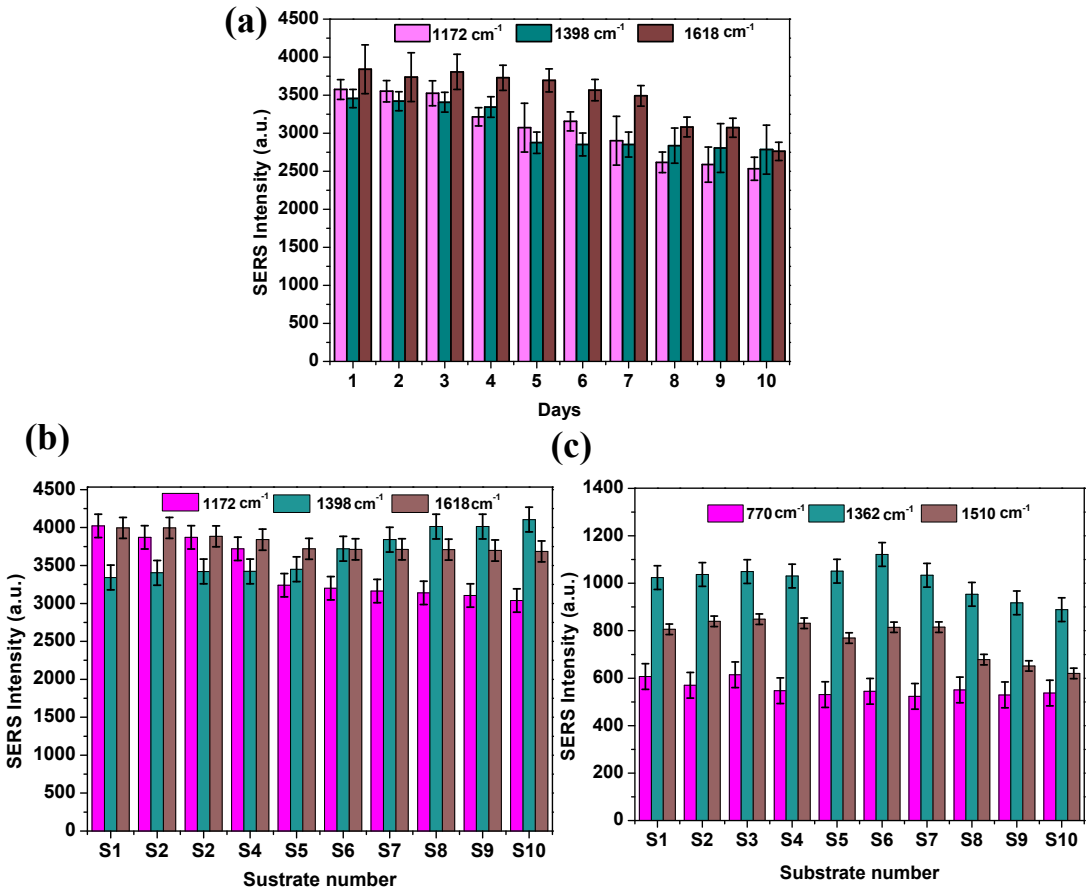

Figure 3.7: (a) Study of the SERS performance with time for the leaf SERS substrate (b) Reproducibility characteristics of MG for ten different substrates with five repetitions for each sample (c) Reproducibility characteristics of R6G for ten different substrates with five repetitions for each sample; (Error bars are plotted using the standard deviation, calculated from five repetitions for each sample)

3.3.7 SERS analysis of the antibiotics

The efficacy of the proposed *AM* SERS substrate has been demonstrated through detecting two antibiotics, CEF-Na and CEFTR, in trace amounts. Stock solutions of 10 ppm were prepared for both CEF-Na and CEFTR by dissolving the required quantity of the analyte in DI water. The stock solutions were then diluted to produce three additional concentrations of CEF-Na and CEFTR (1 ppm, 0.5 ppm, and 0.1 ppm). Figure 3.8(a) shows the SERS signature of CEF-Na as scattered from the proposed leaf SERS substrate. The Raman band assignments for CEF-Na are provided in tabular format in table 8.6 [13]. Regression plots for ten different CEF-Na concentration samples are depicted in figure 3.8(c), with a calculated R^2 of 0.9594. Using the linear regression equation (equation 3.1), it is viable to predict the value of an unknown concentration of the sample.

Table 3.2: Estimation of EF

Analyte	Signature Peak	I_{SERS}	I_{REF}	N_{SERS}	N_{REF}	EF
MG	1398 cm^{-1}	4321 a.u	224 a.u.	2.8137×10^2	3.4021×10^7	2.34×10^6
R6G	1362 cm^{-1}	852 a.u.	220 a.u	1.932×10^2		3.08×10^6

Table 3.3: Comparison of the proposed SERS platform with the already reported SERS substrates

Substrate	Analyte	EF	RSD (%)	LoD (M)	References
Gold deposited plant leaves	Methylene blue	$\sim 10^5$	10	10^{-10}	[10]
	Pyridine	$\sim 10^5$	Not specfied	Not specfied	
Ag coated natural taro-leaf	R6G	10^6	~9.7	10^{-8}	[11]
	furazolidone	Not specfied	Not specfied	Not specfied	
AgNP on dried rose petals	R6G	Not specfied	Not specfied	10^{-9}	[12]
AuNP decorated leaf	MG, R6G, CEF-Na and CEFTR	10^6	10	0.88×10^{-9}	Present work

$$Y = (-0.1587 \pm 0.0239) + (1.0471 \pm 0.0715)X \tag{3.1}$$

Ten different concentrations of CEFTR within the range of 0.1 to 1.0 ppm were prepared in the laboratory. Figure 3.8(b) displays the recorded Raman spectra of four different CEFTR samples scattered from the SERS substrate. The band assignments for CEFTR are provided in table 8.7 in the appendix section [14]. Additionally, Figure 3.8(d) illustrates the characteristic plot of the scattered Raman peak intensity of CEFTR at 1371 cm^{-1} for all ten samples, with R^2 estimated to be 0.9799. Equation 3.2 can be used to predict the concentrations of CEFTR in an unknown sample.

$$Y = (-0.0903 \pm 0.0382) + (1.1104 \pm 0.0528)X \tag{3.2}$$

3.3.8 SERS analysis of the real samples

In the subsequent phase of the current investigation, the detection of CEF-Na and CEFTR in field-collected milk samples was assessed. Following the extraction protocol outlined in Section 3.2.5, milk samples were prepared in the laboratory. The extracted milk samples were then dispensed onto the sensing area of the leaf substrates and dried in a vacuum desiccator for 2 hours. Prior to performing the SERS analysis, the Raman spectra of the background analytes used during the sample extraction process have been recorded and the acquired spectra are depicted in figure 3.8(e). The band assignments for the background chemicals are included in table 8.8 [14]. Figure 3.8(f) illustrates the SERS spectra of the field-collected milk samples. The characteristic Raman bands near 1396 cm^{-1}, 1463 cm^{-1}, and 1584 cm^{-1} confirm

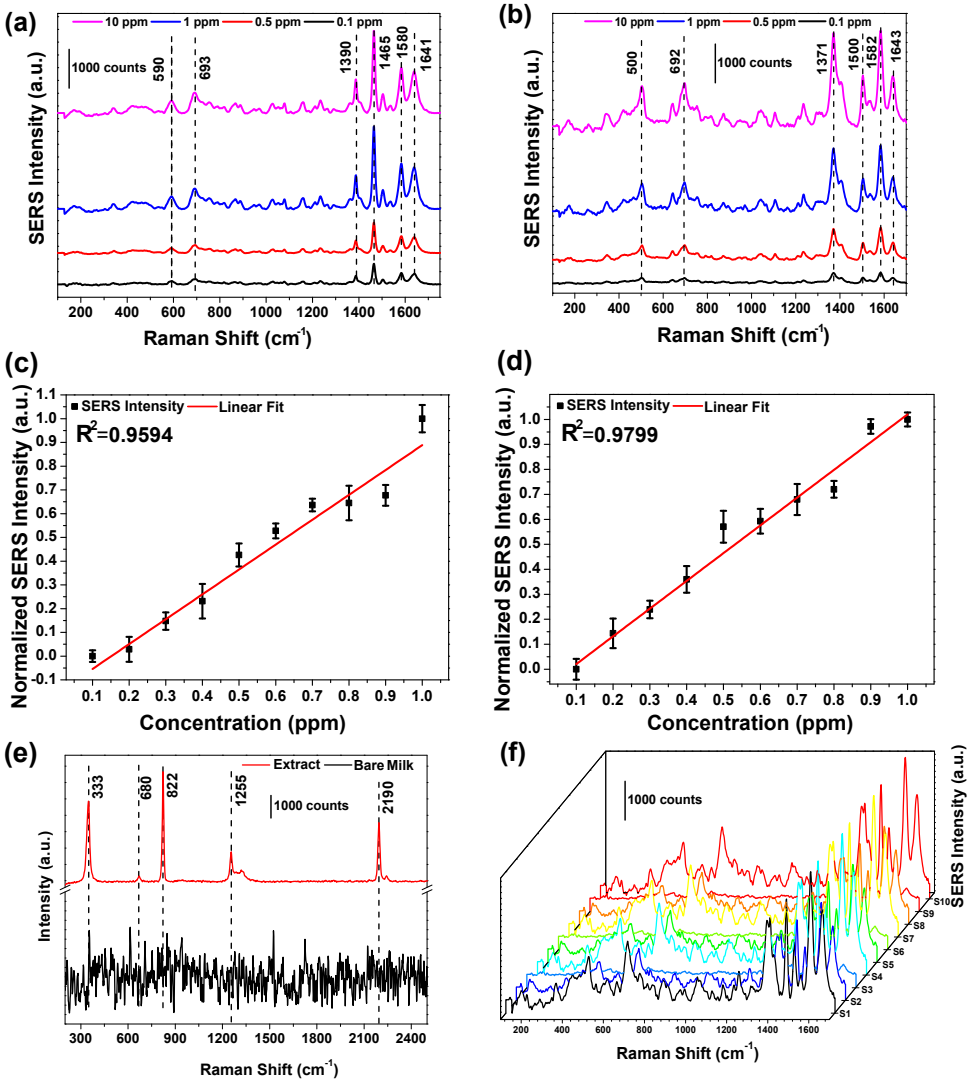

Figure 3.8: Backscattered Raman signal intensity of (a) CEF-Na and (b) CEFTR; linear regression plots of (c) CEF-Na at 1465 cm^{-1} and CEFTR at 1371 cm^{-1} (e) background spectra of the chemicals used for extraction and the Raman spectra of blank milk samples (f) SERS signature of 10 field-collected milk samples (with 7 samples with positive signatures of antibiotics); (Error bars are plotted using the standard deviation, calculated from five repetitions for each sample)

the presence of CEF-Na in the extracted sample. The other peaks of CEF-Na appear to be perturbed in the field-collected milk samples. Similarly, the Raman bands near 496 cm^{-1}, 691 cm^{-1}, 1368 cm^{-1}, 1508 cm^{-1}, and 1642 cm^{-1} confirm the presence of CEFTR in the field-collected milk samples.

3.3.9 Implementation of ML

In the final phase of the present study, a ML model has been developed to classify the two antibiotics present in milk samples. Prior to feeding the data into ML algorithms, PCA was conducted on a dataset comprising 200 milk samples to identify the PCs, that represent the directions of maximum variances. The obtained PCs were

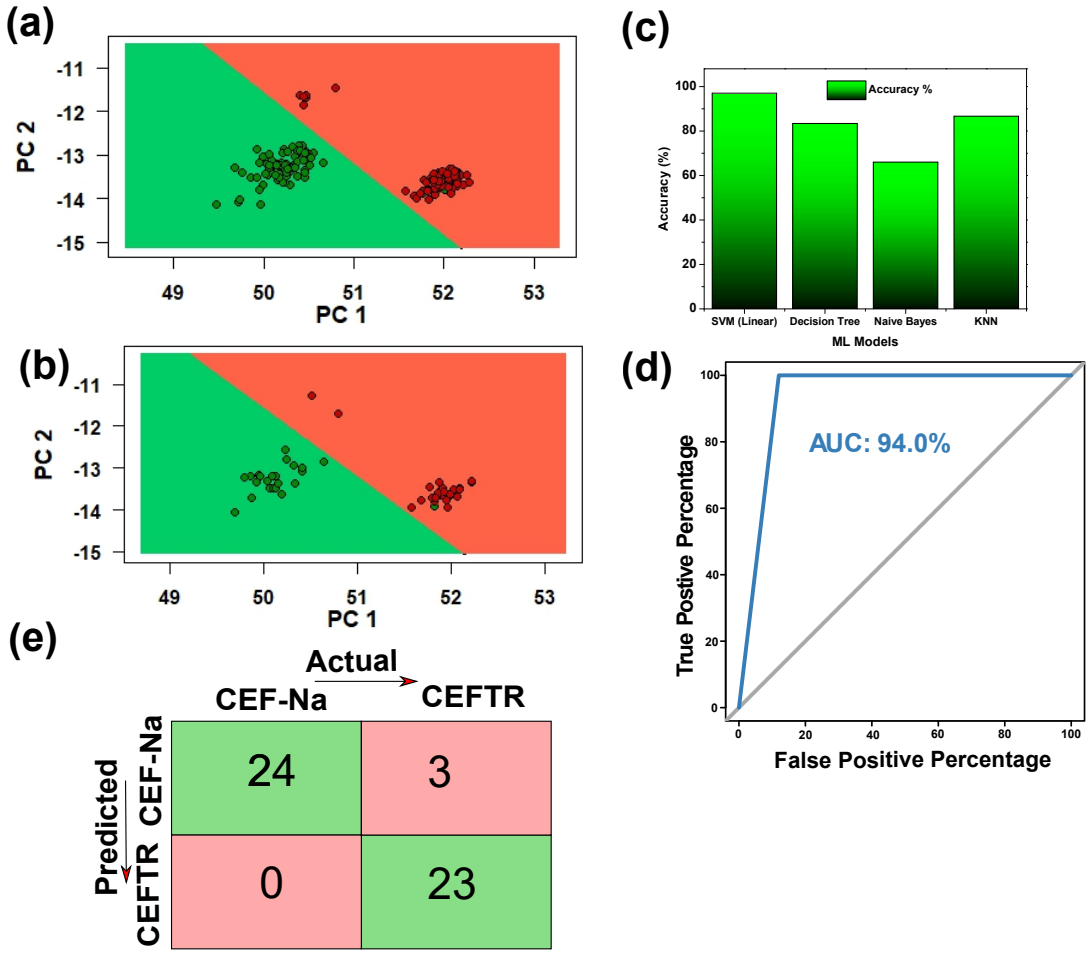

Figure 3.9: Classification of the CEF-Na and CEFTR in the milk samples using SVM classifier for (a) training set (b) test set; (c) Comparison of accuracy percentage for four widely used ML algorithms (d) ROC characteristics of the SVM ML model with AUC 94% (e) the confusion matrix obtained in the present sensing work; (Error bars are plotted using the standard deviation, calculated from five repetitions for each sample)

selected as input for four widely-used ML classification algorithms: SVM, Decision Trees, Naïve Bayes, and KNN. For the ML analysis, the dataset comprised a total of 200 milk samples. This dataset was then split into two subsets: a training set and a test set, in a ratio of 75% (150 samples) to 25% (50 samples). To determine the most suitable algorithm for the current sensing scheme, model parameters such as percentage accuracy and the Area Under the Curve (AUC) in the Receiver Operating Characteristic (ROC) curve were evaluated. Figures 3.9(a) and 3.9(b) display the SVM-based classification plots for the training and test datasets, respectively. These plots demonstrate that the two antibiotic samples can be effectively distinguished using the ML algorithm in combination with PCA, indicating a minimal rate of false positives. Figure 3.9(c) illustrates the comparison of accuracy rates for different ML algorithms employed in the current study. It is evident that SVM coupled with PCA serves as an effective classification model for the present sensing investi-

gations. Figure 3.9(d) depicts the ROC characteristics of the SVM classifier, with an AUC estimated at 94%, indicating a robust classification model for the proposed sensing work. Furthermore, figure 3.9(e) presents the confusion matrix obtained from the SVM classification model. The numbers in the green inset represent correct predictions, while those in the red inset denote incorrect predictions. The confusion matrix revealed 47 correct predictions and 3 incorrect predictions for a training set comprising 50 samples. The ML-based analysis infers that different samples can be segregated with a high accuracy from a mixed sample. Such ML-based SERS signal analysis have been reported in the recent years [15, 16] We envision that the proposed scheme could be extended further for trace detection and quantification of other analyte from complex matrices. With the incorporation of an ML-based regression model, accurate estimation of the concentration can also be performed. Besides the aforementioned approach, feature extraction technique such as linear discriminant analysis (LDA) [15] can be implemented to segment different parameters in a matrix. A proper feature extraction method coupled with an optimized ML model would be explored for other complex matrices and hence serve as a future scope of the present thesis work.

3.4 Summary

The functionality of an *AM* leaf decorated with AuNPs as an alternative SERS platform, exhibiting a notable sensitivity and reproducibility characteristics is demonstrated. With the designed proposed SERS substrate signal enhancement of 10^6 has been achieved. Upon noticing its performance with standard samples, the applicability of the developed platform was showed to detect and quantify residues of two commonly used antibiotics, CEFTR and CEF-Na, in cow milk samples. With the fabricated SERS platform, both targeted antibiotic analytes were detectable at levels compliant with the standards set by FAO. Furthermore, the incorporation of PCA and ML-based classification enhances the overall performance in terms of identifying and categorizing specific analytes within complex mediums. A high degree of percentage accuracy was observed for the targeted samples within the proposed sensing framework.

References

[1] Zhuang, S., Cheng, J., Chen, S., Li, Y., Ding, D., Yu, Z., and Xie, Y. Lotus leaf-inspired biomimetic SERS substrate for detection of thiram on apple. *Food Bioscience*, page 103818, 2024.

[2] Kumar, P., Khosla, R., Soni, M., Deva, D., and Sharma, S. K. A highly sensitive, flexible SERS sensor for malachite green detection based on Ag decorated microstructured PDMS substrate fabricated from Taro leaf as template. *Sensors and Actuators B: Chemical*, 246:477–486, 2017.

[3] Kimling, J., Maier, M., Okenve, B., Kotaidis, V., Ballot, H., and Plech, A. Turkevich method for gold nanoparticle synthesis revisited. *The Journal of Physical Chemistry B*, 110(32):15700–15707, 2006.

[4] Adomaviit, S., Velika, M., and ablinskas, V. Detection of aspirin traces in blood by means of surface-enhanced Raman scattering spectroscopy. *Journal of Raman Spectroscopy*, 51(6):919–931, 2020. Publisher: Wiley Online Library.

[5] Cheng, G., Zhao, J., Wang, X., Yang, C., Li, S., Lu, T., Li, X., Wang, X., and Zhu, G. A highly sensitive and selective method for the determination of ceftiofur sodium in milk and animal-origin food based on molecularly imprinted solid-phase extraction coupled with HPLC-UV. *Food Chemistry*, 347:129013, 2021.

[6] Dhall, D., Kaur, R., and Juneja, M. Machine learning: a review of the algorithms and its applications. *Proceedings of ICRIC 2019: Recent innovations in computing*, pages 47–63, 2020.

[7] Gitelson, A. A., Buschmann, C., and Lichtenthaler, H. K. Leaf chlorophyll fluorescence corrected for re-absorption by means of absorption and reflectance measurements. *Journal of Plant Physiology*, 152(2):283–296, Jan. 1998. ISSN 0176-1617. doi: 10.1016/S0176-1617(98)80143-0. URL https://www.sciencedirect.com/science/article/pii/S0176161798801430.

[8] Israsena Na Ayudhya, T., Posey, F. T., Tyus, J. C., and Dingra, N. N. Using a microscale approach to rapidly separate and characterize three photosynthetic pigment species from fern. *Journal of Chemical Education*, 92(5):920–923, 2015.

[9] Choi, C. J., Xu, Z., Wu, H.-Y., Liu, G. L., and Cunningham, B. T. Surface-enhanced Raman nanodomes. *Nanotechnology*, 21(41):415301, 2010. Number: 41 Publisher: IOP Publishing.

[10] Sharma, V., Kumar, S., Jaiswal, A., and Krishnan, V. Gold deposited plant leaves for SERS: role of surface morphology, wettability and deposition technique in determining the enhancement factor and sensitivity of detection. *ChemistrySelect*, 2(1):165–174, 2017.

[11] Huang, J.-A., Zhang, Y.-L., Zhao, Y., Zhang, X.-L., Sun, M.-L., and Zhang, W. Superhydrophobic SERS chip based on a Ag coated natural taro-leaf. *Nanoscale*, 8(22):11487–11493, 2016. Number: 22.

[12] Xu, B.-B., Zhang, Y.-L., Zhang, W.-Y., Liu, X.-Q., Wang, J.-N., Zhang, X.-L., Zhang, D.-D., Jiang, H.-B., Zhang, R., and Sun, H.-B. Silver-coated rose petal: green, facile, low-cost and sustainable fabrication of a SERS substrate with unique superhydrophobicity and high efficiency. *Adv. Opt. Mater.*, 1(1): 56–60, 2013.

[13] Gunasekaran, S. and Charles, J. Spectral measurements and qualitative analysis of ceftriaxone and cefotaxime. *Asian Journal of Chemistry*, 20(2):1343, 2008. ISSN 0970-7077. Number: 2.

[14] Neelakantan, P. Raman spectrum of acetonitrile. In *Proceedings of the Indian Academy of Sciences-Section A*, volume 60, pages 422–424. Springer, 1964.

[15] Ralbovsky, N. M. and Lednev, I. K. Towards development of a novel universal medical diagnostic method: Raman spectroscopy and machine learning. *Chemical Society Reviews*, 49(20):7428–7453, 2020. Number: 20.

[16] Ding, Y., Sun, Y., Liu, C., Jiang, Q.-Y., Chen, F., and Cao, Y. SERS-Based Biosensors Combined with Machine Learning for Medical Application. *ChemistryOpen*, 12(1):e202200192, 2023.